2008 American Control Conference
Westin Seattle Hotel, Seattle, Washington, USA
June 11-13, 2008

Controller Enhanced Fault Detection and Isolation in a Reactor-Separator System

Benjamin J. Ohran, Johnny Rau, Panagiotis D. Christofides and James F. Davis

Abstract— **Accurate detection and isolation of faults is a critical component of a reliable fault-tolerant control system. In a recent work, it has been demonstrated that using a nonlinear controller to enforce a specific structure in the closed-loop system allows data-based detection and isolation of certain faults that would otherwise not be isolable using data-based techniques without the necessary closed-loop system structure. In this work, we demonstrate through a multi-unit chemical process example how this approach can be applied in a plant-wide setting. Nonlinear, model-based control laws are used to enforce a decoupling structure in the closed-loop system, and data-based statistical process monitoring methods are used for fault detection with isolation of the faults based on the imposed closed-loop system structure.**

I. Introduction

Implementation of a successful fault-tolerant control structure in a chemical process setting requires quick and accurate fault detection and isolation (FDI) [1], [2]. Some of the major difficulties in performing successful fault detection and isolation stem from the fact that most chemical plants are highly nonlinear and frequently have fully coupled dynamics. This makes process behavior hard to predict and makes state responses to different faults generally indistinguishable. Methods of fault detection based on process measurements as developed in the field of statistical process monitoring are fairly reliable and accurate for detecting the presence of a fault [3]. However, fault isolation is a more difficult task. Generally, fault isolation techniques are divided into two categories: model-based and data-based. Model-based techniques rely on a mathematical model of the process to create dynamic filters and compute residuals that directly relate to specific faults. Using the model-based approach, fault isolation can be performed for specific model and fault structures [4]. On the other hand, data-based methods of fault detection and isolation rely exclusively on process measurements. In general, data-based methods require historical data obtained from the system under faulty behavior in order to distinguish between faults. Other methods have been developed that consider the contribution of particular states to the shift from normal operation [5]. Many data-based methods take advantage of principle component analysis (PCA) to more effectively handle large amounts of data or to find relationships within the data [6], [7]. It is also common to group data based on process subsystems or process distinct timescales as in multi-block or multi-scale PCA [8], [9]. While these methods have had varying degrees of success, isolation remains a difficult task, particularly for nonlinear systems where historical data under faulty operation is hard to obtain or are insufficient to discriminate between faults. For a comprehensive review of model-based and data-based fault detection and isolation methods, the reader may refer to [10], [11].

The focus of this work is to demonstrate in a plant-wide setting a recently introduced method of fault detection and isolation that integrates model-based controller design with data-based fault detection in order to perform fault isolation. In [12], the authors demonstrated how a model-based controller could be designed to enhance the isolability of particular faults in the closed-loop system. In this approach, specific faults are partially decoupled from other states in the system in order to create a unique response for individual faults in the system. Data-based process monitoring techniques are used to detect the presence of a fault and to allow isolation based upon the enforced structure within the closed-loop system. This is demonstrated using a multi-unit process consisting of a two CSTR system and a flash tank separator with recycle.

Financial support from NSF, CTS-0529295, is gratefully acknowledged.

The authors are with the Department of Chemical and Biomolecular Engineering, University of California, Los Angeles, CA 90095-1592, USA. Panagiotis D. Christofides is also with the Department of Electrical Engineering, University of California, Los Angeles, CA 90095-1592, USA, ohran@ucla.edu, jrau@ucla.edu, pdc@seas.ucla.edu, jdavis@oit.ucla.edu

II. Preliminaries

A. Fault Signatures

The objective of this paper is to demonstrate the method proposed in [12] of controller enhanced fault detection and isolation in a multi-unit setting. Controller enhanced FDI was introduced in [12] as a method of dividing the state vector into a number of partially decoupled subvectors which can be monitored for their individual responses to particular faults in the system using process measurements only. Based on their responses and the system structure imposed by the model-based controllers, it is possible to discriminate between individual faults or groups of faults. Dividing the state vector into partially decoupled subvectors is accomplished by using model-based control laws to enforce an appropriate structure. First, in order to understand the necessary structure to perform isolation, we review the definitions of the incidence graph, the reduced incidence graph and the isolability graph [12], [13].

Definition 1: The incidence graph of an autonomous system $\dot{x} = f(x)$ with $x \in \mathbb{R}^n$ is a directed graph defined by n nodes, one for each state, $x_i,\ i = 1 \dots n$, of the system. A

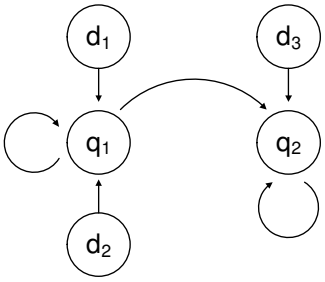

Fig. 1. Isolability graph of the system of Eq.1.

directed arc with origin in node x_i and destination in node x_j exists if and only if $\frac{\partial f_j}{\partial x_i} \neq 0$.

Definition 2: The reduced incidence graph of an autonomous system $\dot{x} = f(x)$ with $x \in \mathbb{R}^n$ is the directed graph of nodes q_i, where $i = 1, ..., N$, that has the maximum number of nodes, N, and satisfies the following conditions:

- To each node q_i there corresponds a set of states $X_i = \{x_j\}$. These sets of states are a partition of the state vector of the system, i.e.,

$$\bigcup X_i = \{x_1, \dots x_n\}, \quad X_i \bigcap X_j = \emptyset, \ \forall i \neq j.$$

- A directed arc with origin q_i and destination q_j exists if and only if $\frac{\partial f_l}{\partial x_k} \neq 0$ for some $x_l \in X_i$, $x_k \in X_j$.
- There are no loops in the graph.

Definition 3: The isolability graph of an autonomous system $\dot{x} = f(x, d)$ with $x \in \mathbb{R}^n$, $d \in \mathbb{R}^p$ is a directed graph made of the N nodes of the reduced incidence graph of the system $\dot{x} = f(x, 0)$ and p additional nodes, one for each possible fault d_k. The graph contains all the arcs of the reduced incidence graph of the system $\dot{x} = f(x, 0)$. In addition, a directed arc with origin in fault node d_k and destination to a state node q_j exists if and only if $\frac{\partial f_l}{\partial d_k} \neq 0$ for some $x_l \in X_j$.

These definitions are convenient in presenting the basic dependencies within a state vector. In most complex systems, the states are fully coupled and the isolability graph contains a single node representing all of the states in the system. However, in systems with partially decoupled dynamics this graph demonstrates graphicly the partially independent subsets of the state vector. Consider, for example, the following system:

$$\begin{aligned} \dot{x}_1 &= -x_1 + x_2 + d_1 \\ \dot{x}_2 &= -x_2 + x_1 + d_2 \\ \dot{x}_3 &= -x_3 + x_1 + d_3 \end{aligned} \tag{1}$$

Because x_1 and x_2 are mutually dependent but are not affected by x_3, they form a partially decoupled subsystem represented by a single node (q_1) in the isolability graph leaving x_3 to form a node by itself (q_2). Figure 1 shows the isolability graph for the system of Eq.1. With the isolability graph of a system, it is possible to consider fault isolation based upon monitoring the subsystems. For this purpose it is necessary to review the definition of a fault signature given below [12]:

Definition 4: The signature of a fault d_k of an autonomous system subject to p faults $\dot{x} = f(x, d)$ with $x \in \mathbb{R}^n$, $d \in \mathbb{R}^p$ is a binary vector W^k of dimension N, where N is the number of nodes of the reduced incidence graph of the system. The i^{th} component of W^k, denoted W^k_i, is equal to 1 if there exists a path in the isolability graph from the node corresponding to fault k to the node q_i corresponding to the set of states X_i, or 0 otherwise.

Using this definition of a fault signature and the isolability graph shown in Figure 1, it is possible to identify the fault signatures for the three faults considered in the system of Eq.1. In this case, because the node $q_2 = \{x_3\}$ does not affect the node $q_1 = \{x_1, x_2\}$, the fault d_3 has the signature $W^3 = [0\ 1]$ and the two faults d_1 and d_2 which affect q_1 and q_2 have the signature $W^1 = W^2 = [1\ 1]$. Based on this, it is expected that a failure in d_1 or d_2 will affect all of the states, whereas a failure in d_3 is expected to affect only those in q_2. In this regard, it is possible to distinguish between a failure in d_3 from a failure in d_1 or d_2 based on the system response. However, it is not generally possible to discriminate between a failure in d_1 and d_2.

B. Process Monitoring

The discussion in the previous section focused on deterministic process behavior in which evaluation of the fault signature based on the isolability graph is straight-forward. On the other hand, in noisy processes, it is possible to have false positives and false negatives in determining the affect of a fault on the state trajectories. In the simulation results section of this paper, autocorrelated process noise is added to the right-hand side of the dynamic process model in Eq.5 and white sensor noise is added to process measurements. For this reason, in order to make a comparison between the fault signature based on the expected response of the system from the isolability graph and the system signature based on the actual behavior, it is necessary to use a method of monitoring the state trajectories that clearly distinguishes normal behavior from faulty behavior and is tolerant to the normal amount of process variation. Additionally, it is assumed that faults of interest will be sufficiently large so that their effect will not be masked by normal process variation.

For the purpose of process monitoring, we use Hotelling's T^2 statistic, a well established method in statistical process control that monitors multivariate data using a single statistic [14]. Because of its suitability for continuous, serially correlated chemical processes, the method of using single measurements is applied [15], [16]. The T^2 statistic is computed using the multivariate state vector (or subset of the state vector) $x \in \mathbb{R}^n$, the expected or desired mean $\bar{x}$ (the normal operating point) and the estimated covariance matrix S obtained using h historical measurements of the system under normal operation:

$$T^2 = (x - \bar{x})^T S^{-1} (x - \bar{x}). \tag{2}$$

The upper control limit for the T^2 statistic is obtained from

its distribution

$$T^2_{UCL} = \frac{(h^2-1)n}{h(h-n)} F_\alpha(n, h-n) \tag{3}$$

where $F_\alpha(n, h-n)$ is the value from the F distribution with $(n, h-n)$ degrees of freedom corresponding to a confidence level α.

The T^2 statistic is used to both detect that a fault has occurred as well as provide the system signature that can be compared with the fault signatures defined in the isolability graph. In order to perform these tasks, the T^2 statistic based on the full state vector x with upper control limit T^2_{UCL} is used to detect the presence of a fault. Additionally, the statistic T^2_i with T^2_{UCLi} where $i = 1, \ldots, N$ that is based on each of the nodes q_i and their corresponding states $x_j \in X_i$ is used to monitor the status of each subset of the state vector.

The fault detection and isolation procedure then follows the steps given below [12]:

1. A fault is detected if $T^2(t) > T^2_{UCL}\ \forall t\ t_f \leq t \leq T_P$ where t_f is the first time T^2 crosses the UCL and T_P is chosen so that the window $T_P - t_f$ is large enough to allow fault isolation within a desired degree of confidence. Choosing T_P depends on the process time constants and potentially on available historical information on the process behavior.
2. A fault that is detected can be isolated if the signature vector of the fault $W(t_f, T_P)$ can be built as follows:

   $$T^2_i(t) > T^2_{UCLi}\ \forall t\ t_f \leq t \leq T_P \rightarrow W_i(t_f, T_P) = 1.$$

   $$T^2_i(t) \not> T^2_{UCLi}\ \forall t\ t_f \leq t \leq T_P \rightarrow W_i(t_f, T_P) = 0.$$

   In such a case, fault d_k is detected at time T_P if $W(t_f, T_P) = W^k$. If two or more faults are defined by the same signature, isolation between them is not possible on the basis of the fault signature obtained from the isolability graph.

Remark 1: In the data-based FDI method presented above, the upper control limit is chosen based on common-cause variance, including process and sensor noise, in order to minimize false alarms. Additionally, to further avoid false alarms, a period of persistent failure is required, $T_P - t_f$. For these reasons, small disturbances or failures are likely to go undetected if the magnitude and effect of the disturbance is on the same level as that of the inherent process variance. Specifically, in order to declare a fault, d_k must be sufficiently large in order for $T^2_i(t)$ to exceed the threshold $T^2_{UCLi}\ \forall t\ t_f \leq t \leq T_P$. Clearly, faults that do not meet the criteria for declaring a fault are, from the point of view of faulty behavior, not of major consequence. However, it should be noted that there is the probability (albeit low) that there is a fault d_k that is large enough to signal a fault in the full state vector, x, but is not large enough to signal a fault in all of the affected subgroups. In this case, it is possible to have a false isolation.

C. Controller Design

This approach to fault detection and isolation can be applied if the signatures of the faults in the closed-loop system are distinct. The uniqueness of a fault depends on the structure of the closed-loop system as shown in the isolability graph. In general, complex nonlinear systems are fully coupled and faults cannot be isolated using the aforementioned method. In order to perform isolation, the closed-loop system structure must be such that the isolability graph has multiple nodes and thus multiple fault signatures. In fully coupled systems, the appropriate structure can be imposed in the closed-loop system in order to make such isolation possible. This can be accomplished implementing a model-based control law that has been appropriately designed to enforce an isolable structure in the closed-loop system. As an example this is demonstrated with the system of Eq.1. Consider a controller added to the right-hand side of the dynamic equation for the state x_1 of the form:

$$u = -x_2 + v$$

where v is an external controller that may be used for stabilizing the system. With this controller, the closed-loop system takes the form:

$$\begin{aligned} \dot{x}_1 &= -x_1 + d_1 + v \\ \dot{x}_2 &= -x_2 + x_1 + d_2 \\ \dot{x}_3 &= -x_3 + x_1 + d_3 \end{aligned} \tag{4}$$

Since there are no longer loops in the system, the reduced incidence graph is now equivalent to the incidence graph having three nodes (one for each state). Consequently, it becomes possible to distinguish between faults d_1 and d_2 using the method described above. This method will be applied to the reactor-separator system described in the next section.

III. Reactor-Separator Process

A. Process Description and Modeling

The process considered in this study is a three vessel, reactor-separator system consisting of two continuously stirred tank reactors (CSTRs) and a flash tank separator [17]. A feed stream to the first CSTR contains the reactant A which is converted into the desired product B. The desired product can then further react into an undesired side-product C. The effluent of the first CSTR along with additional fresh feed makes up the inlet to the second CSTR. The reactions $A \rightarrow B$ and $B \rightarrow C$ (referred to as 1 and 2, respectively) take place in the two CSTRs in series before the effluent from CSTR 2 is fed to a flash tank. The overhead vapor from the flash tank is condensed and recycled to the first CSTR, and the bottom product stream is removed. A small portion of the overhead is purged before being recycled to the first CSTR. All three vessels are assumed to have static holdup. The dynamic equations describing the behavior of the system, obtained through material and energy balances

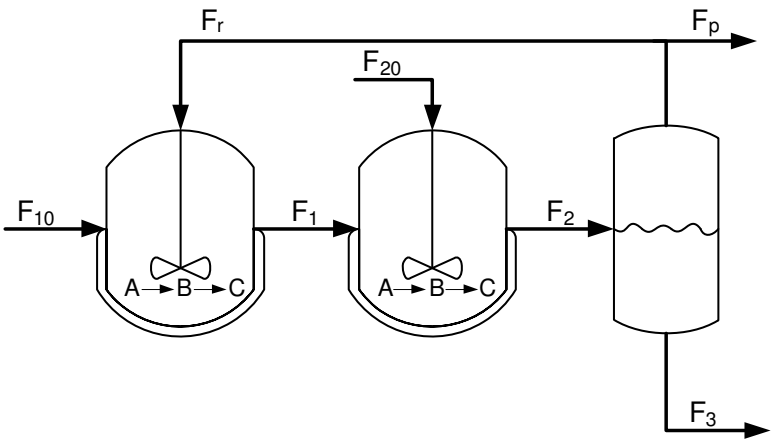

Fig. 2. Reactor-separator system with recycle.

under standard modeling assumptions, are given below.

$$
\begin{aligned}
\frac{dx_{A1}}{dt} &= \frac{F_{10}}{V_1}(x_{A10}-x_{A1})+\frac{F_r}{V_1}(x_{Ar}-x_{A1}) \\
&\quad -k_1 e^{\frac{-E_1}{RT_1}}x_{A1} \\
\frac{dx_{B1}}{dt} &= \frac{F_{10}}{V_1}(x_{B10}-x_{B1})+\frac{F_r}{V_1}(x_{Br}-x_{B1}) \\
&\quad +k_1 e^{\frac{-E_1}{RT_1}}x_{A1}-k_2 e^{\frac{-E_2}{RT_1}}x_{B1} \\
\frac{dT_1}{dt} &= \frac{F_{10}}{V_1}(T_{10}-T_1)+\frac{F_r}{V_1}(T_3-T_1)+\frac{Q_1}{\rho C p V_1} \\
&\quad +\frac{-\Delta H_1}{Cp}k_1 e^{\frac{-E_1}{RT_1}}x_{A1}+\frac{-\Delta H_2}{Cp}k_2 e^{\frac{-E_2}{RT_1}}x_{B1}+u_1 \\
\frac{dx_{A2}}{dt} &= \frac{F_1}{V_2}(x_{A1}-x_{A2})+\frac{F_{20}}{V_2}(x_{A20}-x_{A2}) \\
&\quad -k_1 e^{\frac{-E_1}{RT_2}}x_{A2} \\
\frac{dx_{B2}}{dt} &= \frac{F_1}{V_2}(x_{B1}-x_{B2})+\frac{F_{20}}{V_2}(x_{B20}-x_{B2}) \\
&\quad +k_1 e^{\frac{-E_1}{RT_2}}x_{A2}-k_2 e^{\frac{-E_2}{RT_2}}x_{B2} \\
\frac{dT_2}{dt} &= \frac{F_1}{V_2}(T_1-T_2)+\frac{F_{20}}{V_2}(T_{20}-T_2)+\frac{Q_2}{\rho C p V_2} \\
&\quad +\frac{-\Delta H_1}{Cp}k_1 e^{\frac{-E_1}{RT_2}}x_{A2}+\frac{-\Delta H_2}{Cp}k_2 e^{\frac{-E_2}{RT_2}}x_{B2}+u_2 \\
\frac{dx_{A3}}{dt} &= \frac{F_2}{V_3}(x_{A2}-x_{A3})-\frac{F_r+F_p}{V_3}(x_{Ar}-x_{A3}) \\
\frac{dx_{B3}}{dt} &= \frac{F_2}{V_3}(x_{B2}-x_{B3})-\frac{F_r+F_p}{V_3}(x_{Br}-x_{B3}) \\
\frac{dT_3}{dt} &= \frac{F_2}{V_3}(T_2-T_3)+\frac{Q_3}{\rho C p V_3}
\end{aligned}
\tag{5}
$$

The definitions for the variables used in Eq.5 can be found in Table I, with the parameter values given in Table II. Each of the tanks has an external heat input. In both CSTRs, the heat input is a manipulated variable for controlling the reactors at the appropriate operating temperature. These are the only control actuators considered in the system. The model of the flash tank separator operates under the assumption that the relative volatility for each of the species remains

TABLE I

PROCESS VARIABLES

x_{A1}, x_{A2}, x_{A3}	mass fractions of A in vessels 1, 2, 3
x_{B1}, x_{B2}, x_{B3}	mass fractions of B in vessels 1, 2, 3
x_{C1}, x_{C2}, x_{C3}	mass fractions of C in vessels 1, 2, 3
x_{Ar}, x_{Br}, x_{Cr}	mass fractions of A, B, C in the recycle
T_1, T_2, T_3	temperatures in vessels 1, 2, 3
T_{10}, T_{20}	feed stream temp. to vessels 1, 2
F_1, F_2, F_3	effluent flow rate from vessels 1, 2, 3
F_{10}, F_{20}	feed stream flow rate to vessels 1, 2
F_r, F_p	flow rates of the recycle and purge
V_1, V_2, V_3	volume of vessels 1, 2, 3
u_1, u_2	manipulated inputs
E_1, E_2	activation energy for reactions 1, 2
k_1, k_2	pre-exponential values for reactions 1, 2
ΔH_1, ΔH_2	heats of reaction for reactions 1, 2
α_A, α_B, α_C	relative volatilities of A, B, C
Q_1, Q_2, Q_3	heat input into vessels 1, 2, 3
C_p, R	heat capacity and gas constant

constant within the operating temperature range of the flash tank. This assumption allows calculating the mass fractions in the overhead based upon the mass fractions in the liquid portion of the vessel. It has also been assumed that there is a negligible amount of reaction taking place in the separator. The following algebraic equations model the composition of the overhead stream relative to the composition of the liquid holdup in the flash tank:

$$
\begin{aligned}
x_{Ar} &= \frac{\alpha_A x_{A3}}{\alpha_A x_{A3}+\alpha_B x_{B3}+\alpha_C x_{C3}} \\
x_{Br} &= \frac{\alpha_A x_{B3}}{\alpha_A x_{A3}+\alpha_B x_{B3}+\alpha_C x_{C3}} \\
x_{Cr} &= \frac{\alpha_A x_{C3}}{\alpha_A x_{A3}+\alpha_B x_{B3}+\alpha_C x_{C3}}
\end{aligned}
\tag{6}
$$

The open-loop system of Eq.5 is fully coupled and is represented by a single node in the reduced incidence graph. However, using appropriately designed model-based nonlinear state feedback control laws for the manipulated inputs u_1 and u_2, it is possible to separate the closed-loop system into four nodes in the isolability graph. Consider the following nonlinear control laws which decouple the full state vector

TABLE II

PARAMETER VALUES

$T_{10} = 300$, $T_{20} = 300$	K
$F_{10} = 1.4 \cdot 10^{-3}$, $F_{20} = 1.4 \cdot 10^{-3}$	$\frac{m^3}{s}$
$F_r = 1.4 \cdot 10^{-2}$, $F_p = 1.4 \cdot 10^{-3}$	$\frac{m^3}{s}$
$V_1 = 1.0$, $V_2 = 0.5$, $V_3 = 1.0$	m^3
$E_1 = 5 \cdot 10^4$, $E_2 = 6 \cdot 10^4$	$\frac{J}{mol}$
$k_1 = 2.77 \cdot 10^3$, $k_2 = 2.510^3$	$\frac{1}{s}$
$\Delta H_1 = -6 \cdot 10^4$, $\Delta H_2 = -7 \cdot 10^4$	$\frac{J}{mol}$
$C_p = 4.2 \cdot 10^3$	$\frac{J}{kgK}$
$R = 8.314$	$\frac{J}{molK}$
$\rho = 1000$	$\frac{kg}{m^3}$
$Q_1 = 3.5 \cdot 10^5$, $Q_2 = 4.5 \cdot 10^5$, $Q_3 = 3.5 \cdot 10^5$	$\frac{J}{s}$
$\alpha_A = 3.5$, $\alpha_B = 1$, $\alpha_C = 0.5$	unitless

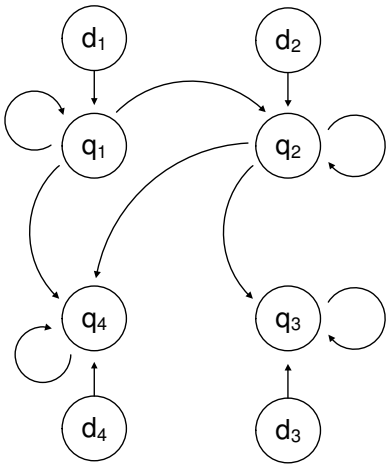

Fig. 3. Isolability graph for the reactor-separator system.

into 4 subvectors [18]:

$$\begin{aligned} u_1 &= \frac{F_r}{V_1}(T_{3ss} - T_3) + \frac{\Delta H_1}{Cp} k_1 e^{\frac{-E_1}{RT_1}}(x_{A1} - x_{A1ss}) \\ &\quad + \frac{\Delta H_2}{Cp} k_2 e^{\frac{-E_2}{RT_1}}(x_{B1} - x_{B1ss}) + v_1 \\ u_2 &= \frac{\Delta H_1}{Cp} k_1 e^{\frac{-E_1}{RT_2}}(x_{A2} - x_{A2ss}) \\ &\quad + \frac{\Delta H_2}{Cp} k_2 e^{\frac{-E_2}{RT_2}}(x_{B2} - x_{B2ss}) + v_2 \end{aligned} \tag{7}$$

where the subscript ss refers to values at the steady state, or set point. The terms v_1 and v_2 are external controllers used to stabilize the system and achieve offset-free output tracking and are defined, according to standard proportional-integral control formulas, as follows:

$$\begin{aligned} v_1(t) &= K_1(T_{1ss} - T_1 + \frac{1}{\tau_{I1}} \int_0^t (T_{1ss} - T_1)dt) \\ v_2(t) &= K_2(T_{2ss} - T_2 + \frac{1}{\tau_{I2}} \int_0^t (T_{2ss} - T_2)dt) \end{aligned} \tag{8}$$

where K_1, K_2 are the proportional controller gains and τ_{I1} and τ_{I2} are the integral time constants. The closed-loop system operating under the control laws defined in Eqs.7-8 decouples T_1 from x_{A1}, x_{B1} and T_3 and T_2 from x_{A2} and x_{B2}. The four subgroups created by the controller of Eqs.7-8 are $q_1 = \{T_1\}$, $q_2 = \{T_2\}$, $q_3 = \{T_3\}$ and $q_4 = \{x_{A1}, x_{A2}, x_{A3}, x_{B1}, x_{B2}, x_{B3}\}$. The resulting isolability graph is shown in Figure 3. From the isolability graph the fault signatures can be defined as follows:

$$\begin{aligned} W^1 &= [1;1;1;1] \\ W^2 &= [0;1;1;1] \\ W^3 &= [0;0;1;0] \\ W^4 &= [0;0;0;1] \end{aligned} \tag{9}$$

The four faults shown in Figure 3 are those that will be considered in this example. They represent failures in the heat inputs to each of the tanks (faults d_1, d_2, d_3) and a feed stream concentration disturbance in species A in the inlet to CSTR 1 (d_4). These are added to the right-hand side of the dynamic equations for T_1, T_2, T_3 and x_{A1}. For comparison purposes, in the simulation results, a PI controller with the form given in Eq.8 is used. This control law is used for comparing the isolability of faults, using process measurements only, in the closed-loop system under PI-only control and in the closed-loop system under the nonlinear feedback control which enforces the isolable structure. Although a PI controller is used for comparison in this work, any controller that does not enforce an isolable structure in the closed-loop system would yield similarly indistinguishable faults. Additionally, the PI-only controller will be used to evaluate the additional cost incurred by the nonlinear feedback controller in order to enforce an isolable structure in the closed-loop system.

B. Simulation Results

The model presented in Section III-A was numerically simulated using a standard Runge-Kutta integration method. The system was modeled with both process and sensor noise. The sensor measurement noise was generated as Gaussian distributed random noise with standard deviation σ_m and was added to the state measurement at a sample rate of 0.1 sample/second. Noisy measurements were used in updating the feedback control law described in Eqs.7-8 on the same interval. Process noise was added to the right-hand side of each equation in the system of ODEs found in Eq.5. Process noise was generated as autocorrelated noise of the form $w_k = \phi w_{k-1} + \xi_k$ where $k = 0, 1, \ldots$ is the discrete time step of 1 second, w_k is a normally distributed random variable with standard deviation σ_p and ϕ is the autocorrelation factor. Table III contains the parameters used in generating the noise. The sensor measurement and process noise were generated independently for each state in the system. For purposes of fault detection, a window of 30 seconds was used in declaring a fault (i.e., $T_P - t_f = 30\ sec$).

The controllers were designed as shown in Eqs.7-8 using control parameters $K_1 = K_2 = \frac{0.01}{sec}$ and $\tau_{I1} = \tau_{I2} = 300sec$. The PI controllers shown for comparison used the

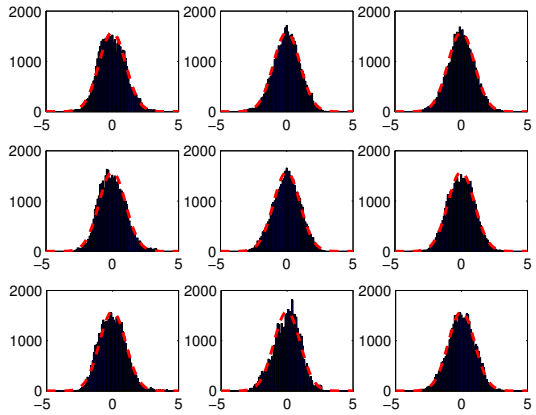

Fig. 4. Normalized histogram plots of each of the system states compared with a normal distribution (dashed) for a large number of measurements during fault-free operation under nonlinear feedback control

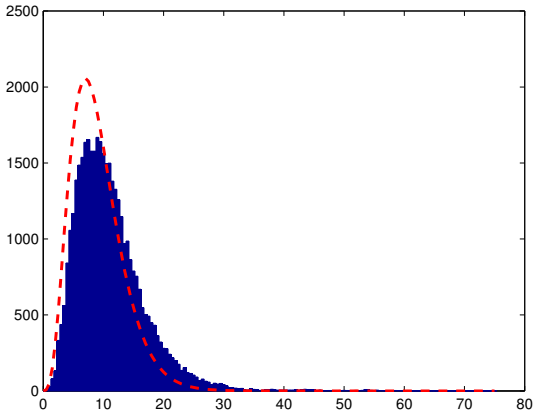

Fig. 5. Histogram of T^2 statistic for the full state vector compared with the expected T^2 distribution (dashed) for a large number of measurements during fault-free operation under nonlinear feedback control

same parameters. The system was controlled at the set point values of $T_{1ss} = 436.8\ K$ and $T_{2ss} = 433.9\ K$. In all cases, the system was initially at steady-state and was simulated for 30 min fault-free and for 30 min after the occurrence of the fault. The four faults were introduced as added terms on the right-hand side of the ODEs in Eq.5; only a single fault was applied in each simulation. The values $d_1 = 1\frac{K}{s}$, $d_2 = 2\frac{K}{s}$, $d_3 = 1\frac{K}{s}$ and $d_4 = -2 \cdot 10^{-3}\frac{1}{s}$ were added to the dynamic equations for T_1, T_2, T_3 and x_{A1}, respectively. These represent changes in the heat input (actuator/valve failures) for faults d_1, d_2 and d_3 and an inlet concentration disturbance in species A for fault d_4. However, these faults could also be thought of as any general faults as the development of this method does not limit the values that d can take.

Four simulation scenarios were carried out, one for each fault, to demonstrate the method of detecting and isolating faults in the closed-loop system. In order to apply the method of fault detection and isolation presented in the preliminaries, the data should be multivariate normal and fit the T^2 distribution under closed-loop operation. Figure 4 demonstrates that the measurements from each of the states closely approximates a Gaussian distribution. The distribution for the measured T^2 values is shown in Figure 5. Again we see that the measured statistic closely approximates the predicted distribution, however, in this case the fit is less exact due to correlation between states. Nonetheless, the distribution is reasonably close. If necessary, the upper control limit can be adjusted upward to provide a more conservative limit if false alarms are problem.

Figure 6 shows the trajectories of the mass fractions in each of the tanks and the recycle stream for the simulation in closed-loop operation under the nonlinear feedback controller with a failure in d_1. The effects of the failure at time $t = 0.5\ hr$ are visible in the plot. The temperature trajectories for each of the tanks is shown in Figure 7 along with the control action requested. Once the failure is

TABLE III

NOISE PARAMETERS

	σ_m	σ_p	ϕ
x_{A1}	1E-3	1E-3	0.7
x_{B1}	1E-3	1E-3	0.7
T_1	1E-3	1E-2	0.7
x_{A2}	1E-3	1E-3	0.7
x_{B2}	1E-3	1E-3	0.7
T_2	1E-3	1E-2	0.7
x_{A3}	1E-3	1E-3	0.7
x_{B3}	1E-3	1E-3	0.7
T_3	1E-3	1E-2	0.7

detected at $t = 0.5\ hr$, the T_i^2 plots are used to determine the fault signature for the system. Figure 8 shows the T^2 statistic results for the four subsets of the state vector as well as for the full state vector. The fault is detected at time $t = 0.5\ hr$ by the full T^2 and is isolated based on the four T_i^2 corresponding to the subsets. Based on the T_i^2 plots the signature of the system in this case is $W = [1; 1; 1; 1] \equiv W^1$. Thus, the fault is correctly isolated as one affecting the states in $q_1 = T_1$, or d_1. Note that although the process data are serially correlated on a short timescale, this was compensated for by using a large amount of historical data for estimating S. Additionally, it has been found that feedback control makes the closed-loop system data more normally distributed (see [16]). Thus, the assumption that the data are multivariate normal for applying the T^2 statistic is reasonable. This was also confirmed in Figures 4-5. The simulation with a failure in d_1 was repeated using only a PI controller for comparison. The states were similarly all affected by fault d_1 (Figure omitted for brevity) and the control action requested was of comparable magnitude with that of the nonlinear feedback controller (see Figure 9). This demonstrates that the control action requested by the nonlinear feedback control law to enforce an isolable structure is not excessive in this case. For the PI controller, the states of the closed-loop system are all fully coupled and thus the state trajectories will all be affected by any fault, making it impossible to distinguish

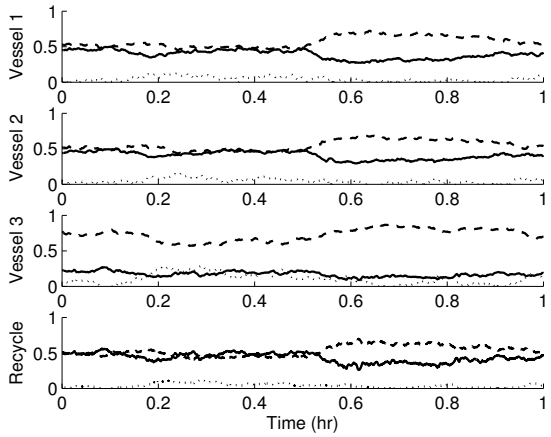

Fig. 6. Plots of the mass fractions x_A (solid), x_B (dashed) and x_C (dotted) for the system under nonlinear feedback control with a failure in d_1 at $t = 0.5\ hr$.

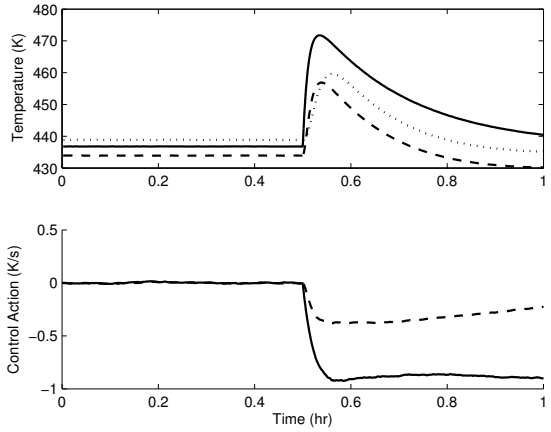

Fig. 7. (top) Temperature trajectories for T_1 (solid), T_2 (dashed) and T_3 (dotted) for the system under nonlinear feedback control with a failure in d_1 at $t = 0.5\ hr$. (bottom) Control action requested for the same system for u_1 (solid) and u_2 (dashed).

between faults on the basis of process measurements. The simulation with a failure in d_2, below, demonstrates this point.

Figure 10 shows the T^2 results for the simulation in closed-loop operation under the nonlinear feedback controller with a failure in d_2 occurring at $t = 0.5\ hr$. Note that although there may be a brief violation of the upper control limit (e.g., at approximately $t = 0.2\ hr$ in Figure 10), this is not declared as a fault nor is it a false alarm since a fault is declared only after a persistent state of failure lasting at least 30 seconds to avoid such situations. Once the fault is declared around time $t = 0.5\ hr$ the signature of the system can be determined from the T_i^2 plots which show $W = [0; 1; 1; 1] \equiv W^2$. For the PI-only controller, all of the states were affected as they were in the case with a failure in d_1; however, the case with the nonlinear feedback controller designed to enforce an isolable structure correctly shows that T_1 is decoupled from the fault, making it possible to isolate.

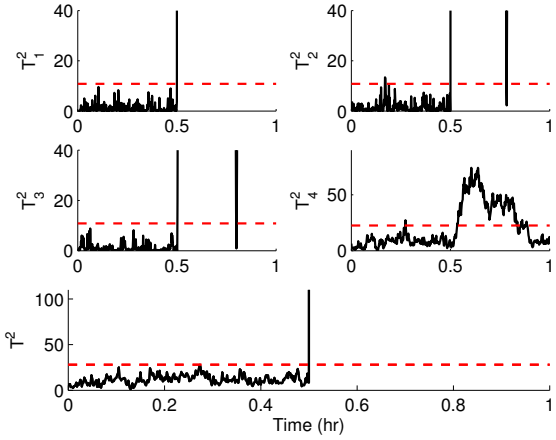

Fig. 8. Plots of the T^2 statistic (solid) with the corresponding T^2_{UCL} (dashed) for each of the subsystems and for the full state vector under nonlinear feedback control with a failure in d_1 at $t = 0.5\ hr$.

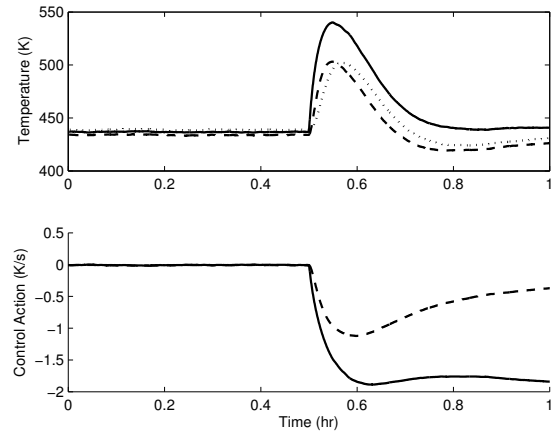

Fig. 9. (top) Temperature trajectories for T_1 (solid), T_2 (dashed) and T_3 (dotted) for the system under PI-only control with a failure in d_1 at $t = 0.5\ hr$. (bottom) Control action requested for the same system for u_1 (solid) and u_2 (dashed).

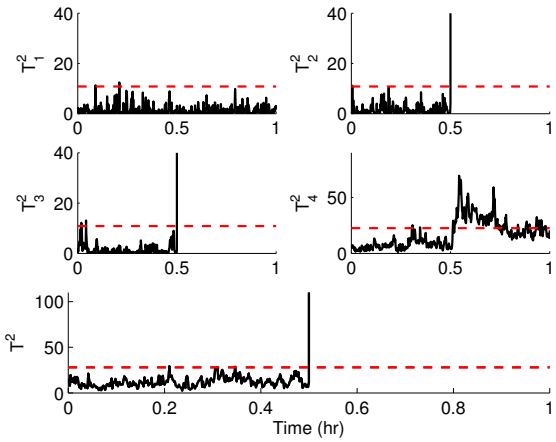

Fig. 10. Plots of the T^2 statistic (solid) with the corresponding T^2_{UCL} (dashed) for each of the subsystems and for the full state vector under nonlinear feedback control with a failure in d_2 at $t = 0.5\ hr$.

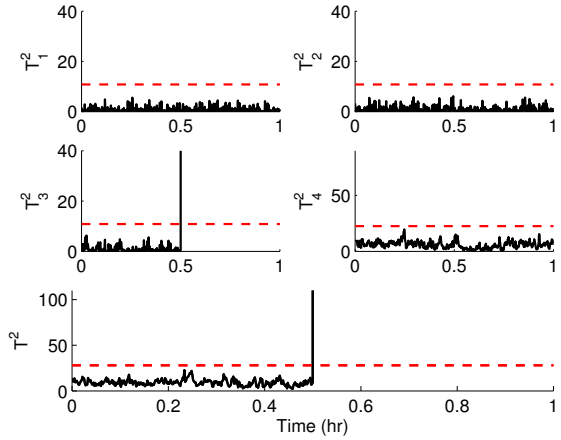

Fig. 11. Plots of the T^2 statistic (solid) with the corresponding T^2_{UCL} (dashed) for each of the subsystems and for the full state vector under nonlinear feedback control with a failure in d_3 at $t = 0.5\ hr$.

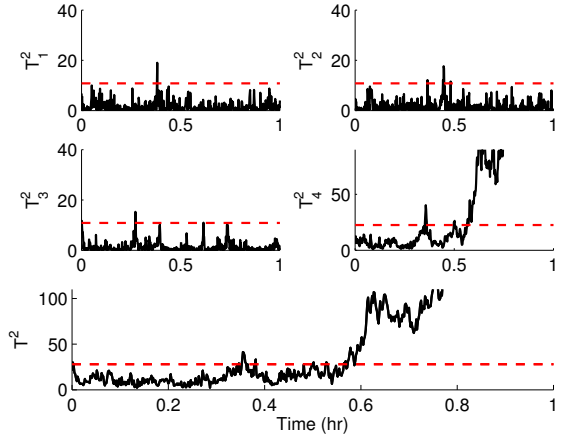

Fig. 12. Plots of the T^2 statistic (solid) with the corresponding T^2_{UCL} (dashed) for each of the subsystems and for the full state vector under nonlinear feedback control with a failure in d_4 at $t = 0.5\ hr$.

The T^2 plots for the system under nonlinear feedback control with a failure in d_3 are shown in Figure 11. This also shows the expected behavior corresponding to the fault signatures defined in Eq.9; that is, the fault affected only the temperature of the flash tank and did not influence the other states. The PI comparison (omitted) showed similar results as before in that all states were affected and a fault could not be isolated based on measured data. Finally, note that for the system under nonlinear feedback control with a failure in d_4 (see Figure 12), the fault signature only shows that the fault affects the dynamics of the states in $q_4 = \{x_{A1}, x_{A2}, x_{A3}, x_{B1}, x_{B2}, x_{B3}\}$. In this case the fault signature indicates that there is a fault in d_4, but is unable to distinguish between any of the faults that directly affect the states within this set.

IV. Conclusions

This work has demonstrated the application of a model-based nonlinear controller designed to enforce an isolable structure in the closed-loop system of a multi-unit reactor-separator chemical process. Fault detection and isolation were performed using statistical process monitoring techniques and information based upon the imposed closed-loop system structure. This was demonstrated through numerical simulation studies of the closed-loop system in the presence of four different faults. It was shown that by decoupling faults of interest from certain states, it was possible to achieve unique system responses to each of the four faults allowing fault isolation based on process measurements only.

References

[1] P. Mhaskar, A. Gani, N. H. El-Farra, C. McFall, P. D. Christofides, and J. F. Davis, "Integrated fault detection and fault-tolerant control of process systems," *AIChE Journal*, vol. 52, pp. 2129–2148, 2006.

[2] P. Mhaskar, A. Gani, and P. D. Christofides, "Fault-tolerant control of nonlinear processes: Performance-based reconfiguration and robustness," *International Journal of Robust & Nonlinear Control*, vol. 16, pp. 91–111, 2006.

[3] S. J. Qin, "Statistical process monitoring: basics and beyond," *Journal of Chemometrics*, vol. 17, pp. 480–502, 2003.

[4] P. Mhaskar, C. McFall, A. Gani, P. Christofides, and J. Davis, "Isolation and handling of actuator faults in nonlinear systems," *Automatica*, vol. 44, pp. 53–62, 2008.

[5] T. Kourti and J. MacGregor, "Multivariate SPC methods for process and product monitoring," *Journal of Quality Technology*, vol. 28, pp. 409–428, 1996.

[6] J. Gertler, L. Weihua, Y. Huang, and T. McAvoy, "Isolation enhanced prinicpal component analysis," *AIChE Journal*, vol. 45, pp. 323–334, 1999.

[7] S. Yoon and J. MacGregor, "Fault diagnosis with multivariate statistical models part I: using steady state fault signatures," *Journal of Process Control*, vol. 11, pp. 387–400, 2001.

[8] J. A. Westerhuis, T. Kourti, and J. F. MacGregor, "Analysis of multiblock and hierarchical PCA and PLS models," *Journal of Chemometrics*, vol. 12, pp. 301–321, 1998.

[9] B. R. Bakshi, "Multiscale PCA with application to multivariate statistical process monitoring," *AIChE Journal*, vol. 44, pp. 1596–1610, 1998.

[10] V. Venkatasubramanian, R. Rengaswamy, K. Yin, and S. Kavuri, "A review of process fault detection and diagnosis part I: Quantitative model-based methods," *Computers and Chemical Engineering*, vol. 27, pp. 293–311, 2003.

[11] V. Venkatasubramanian, R. Rengaswamy, S. Kavuri, and K. Yin, "A review of process fault detection and diagnosis part III: Process history based methods," *Computers and Chemical Engineering*, vol. 27, pp. 327–346, 2003.

[12] B. J. Ohran, D. Muñoz de la Peña, P. D. Christofides, and J. F. Davis, "Enhancing data-based fault isolation through nonlinear control," *AIChE Journal*, vol. 54, pp. 223–241, 2008.

[13] P. Daoutidis and C. Kravaris, "Structural evaluation of control confiurations for multivariable nonlinear processes," *Chemical Engineering Science*, vol. 47, pp. 1091–1107, 1991.

[14] J. Romagnoli and A. Palazoglu, *Introduction to Process Control*. CRC Press, 2006.

[15] N. D. Tracy, J. C. Young, and R. L. Mason, "Multivariate control charts for individual observations," *Journal of Quality Technology*, vol. 24, pp. 88–95, 1992.

[16] D. C. Montgomery, *Introduction to statistical quality control*. John Wiley & Sons, 1996.

[17] A. N. Venkat, J. B. Rawlings, and S. J. Wright, "Stability and optimality of distributed, linear model predictive control Part I: state feedback," in *Texas-Wisconsin Modeling and Control Consortium Technical Report*, vol. 3, 2006.

[18] P. D. Christofides and N. H. El-Farra, *Control of Nonlinear and Hybrid Process Systems: Designs for Uncertainty, Constraints and Time-Delays*, 446 pages. New York: Springer, 2005.